Comparison of spatially and temporally resolved diffuse-reflectance measurement systems for determination of biomedical optical properties

Johannes Swartling, Jan S. Dam, and Stefan Andersson-Engels

Time-resolved and spatially resolved measurements of the diffuse reflectance from biological tissue are two well-established techniques for extracting the reduced scattering and absorption coefficients. We have performed a comparison study of the performance of a spatially resolved and a time-resolved instrument at wavelengths 660 and 785 nm and also of an integrating-sphere setup at 550–800 nm. The first system records the diffuse reflectance from a diode laser by means of a fiber bundle probe in contact with the sample. The time-resolved system utilizes picosecond laser pulses and a single-photon-counting detection scheme. We extracted the optical properties by calibration using known standards for the spatially resolved system, by fitting to the diffusion equation for the time-resolved system, and by using an inverse Monte Carlo model for the integrating sphere. The measurements were performed on a set of solid epoxy tissue phantoms. The results showed less than 10% difference in the evaluation of the reduced scattering coefficient among the systems for the phantoms in the range 9–20 cm^{-1}, and absolute differences of less than 0.05 cm^{-1} for the absorption coefficient in the interval 0.05–0.30 cm^{-1}.

OCIS codes: 120.3150, 120.5820, 170.3890, 170.1470.

1. Introduction

Measuring the optical properties of biological tissue has grown into a mature procedure in the field of biomedical optics. Knowing the light-scattering and absorption properties of tissue is the basis of a wide range of both diagnostic and therapeutic applications. Examples include laser-induced fluorescence to diagnose malignant tissue[1,2] as well as laser-induced hyperthermia[3,4] and photodynamic therapy[5,6] to treat diseased tissue. Novel techniques for optical analysis of deep structures, based on so-called optical tomography, are also being developed.[7,8] The goal of such methods is to obtain spatial maps of the optical properties of the tissue volume. In the development of these techniques, for validation purposes it is important to be able to accurately measure optical properties locally. Small sampling volumes must then be used in which the tissue can be regarded as homogeneous.

A number of techniques to measure the local optical properties of tissue have been developed. Common to most methods is measurement of the diffuse reflectance, and in some cases transmittance, from a sample of the tissue either *in vitro* or *in vivo*. The data are then related to the optical properties by means of a suitable inverse algorithm based either on a theoretical light-propagation model or on calibration by use of standards with known scattering and absorption properties. When spatially resolved reflectance measurements are performed, the sample is illuminated by a cw light source in a spot, and the diffuse reflectance is recorded at different radial distances.[9–15] Time-resolved measurements, however, utilize subnanosecond pulses from a laser. After a pulse has passed passing through a portion of the tissue, its time dispersion can be measured.[16–23] Both of these methods are two-parameter techniques; i.e., the extracted properties are absorption coefficient μ_a' and reduced scattering coefficient μ_s'.

Even though measurements of these two types are now common in biomedical optics, to our knowledge no systematic investigation to experimentally compare the performance of various systems seems to have been made. We have evaluated the perfor-

The authors are with the Department of Physics, Lund Institute of Technology, P.O. Box 118, SE-22100 Lund, Sweden. J. Swartling's e-mail address is johannes.swartling@fysik.lth.se

Received 4 November 2002; revised manuscript received 21 April 2003.

0003-6935/03/224612-09$15.00/0

mance of a spatially resolved and of a time-resolved system on the same samples. In addition, we compared the results with those from integrating-sphere measurements, which are known to give accurate results for *in vitro* samples.[5,24–27] When a measurement of the collimated transmittance is added to the integrating-sphere measurements, this technique becomes a three-parameter method and permits the determination of μ_a, scattering coefficient μ_s, and scattering anisotropy factor g. Reduced scattering coefficient μ_s' is defined as $\mu_s' = (1 - g)\mu_s$.

Our aim in this study was to compare the results and investigate the limitations of the three systems. Inhomogeneous samples are also discussed. In each of the following three sections, one of the three systems is briefly described, with references to publications in which thorough descriptions of the technical details and the data-evaluation methods may be found. Next, data from a phantom study and *in vivo* measurements are presented.

2. Spatially Resolved Diffuse Reflectance System

A. Fiber-Probe System

The fiber-probe system was extensively described in Ref. 15. The system was designed with real-time measurements of the skin surface in a clinical environment in mind. It consists of a probe head with a 200-μm source fiber in the center surrounded by five equally spaced concentric rings of 250-μm detector fibers. Light from four replaceable low-power diode lasers is coupled into the source fiber. The diode lasers may be selected arbitrarily to suit different applications. In the research reported in this paper, diode lasers at wavelengths of 660 and 785 nm (with output powers of 2 mW at the probe head) were used. The fibers of each single ring of detector fibers are bundled and terminated on a separate silicon photodiode for each ring. In addition, three photodiodes and a temperature sensor are mounted directly near the perimeter of the probe head. Thus, diffuse reflectance $R(r)$ can be collected at six distances, i.e., $r =$ 0.6, 1.2, 1.8, 2.4, 3.0, 7.8 mm. Furthermore, a separate reference detector monitors the output of the source fiber at the probe head. Data acquisition and storage are controlled by a laptop PC connected to a digital signal processing board. One cycle of four successive measurements (i.e., one at each wavelength) including dark measurements can be performed in ~10 ms; thus the maximum sampling rate of the system is ~100 Hz. To minimize any interference from background light or drift of the light source, the dark measurements are subtracted from the measured reflectance data, after which they are normalized relative to the source reference. The digital signal processing board accomplishes this before the data are analyzed, displayed, and stored by the PC.

B. Calibration and Prediction Algorithms

Because the unknown numerical apertures of the fiber-probe light source and detectors were not know the system was calibrated directly on a set of phantoms instead of by use of a mathematical light-propagation model. The phantoms consisted of epoxy resin with well-defined quantities of TiO and absorbing pigment added for scattering and absorption, respectively. The scattering and absorption spectra were determined from integrating-sphere measurements. A set of 72 calibration phantoms was used, with 8 different scatterer concentrations and 9 different absorber concentrations. The calibration phantoms were prepared in the same way as the validation set described below in Section 5. The ranges of optical properties used in the calibration phantoms were, at 660 nm, $0.01 < \mu_a < 0.5$ and $4.5 < \mu_s' < 25\ \text{cm}^{-1}$. At 785 nm the ranges were $0.05 < \mu_a < 0.5$ and $4.0 < \mu_s' < 20\ \text{cm}^{-1}$.

In theory, μ_a and μ_s' can be determined by use of $R(r)$ data from only two of the six detector distances of the fiber probe. However, to reduce the influence of tissue inhomogeneity and of noisy measurement conditions we included the signals from all source–detector distances in the analysis. We did this for each measurement by first applying principal-component analysis to the data from all six source–detector distances of the probe system and then using the resultant weight coefficients for the two main principal components, P_1 and P_2, in the analysis.P_1 and P_2 from all phantoms were then fitted to two-dimensional polynomials by least-squares regression to create a calibration model to extract μ_a and μ_s' from the spatially resolved measurements in the same way as described in Ref. 15 We call this technique the multiple polynomial regression (MPR) method. The next step was to solve the inverse problem of determining μ_a and μ_s' from $R(r)$ measurements of a set of prediction samples. We did this by employing a two-dimensional Newton–Raphson algorithm of the two principal components from each measurement.

3. Time-Resolved System

A. Instrument for Time-Resolved Measurements

Picosecond pulsed diode lasers at 660 and 785 nm (SEPIA; PicoQuant GmbH, Germany) were used as light sources. The light was brought to the sample by a 50-μm-diameter gradient-index optical fiber. A 600-μm-diameter fiber was used to collect the diffusely reflected light and guide it to the detector, a microchannel plate-photomultiplier tube (R2566U; Hamamatsu Photonics K. K., Japan). A time-correlated single-photon-counting technique[17] was employed to record the time-dispersion curves. To this end, an SPC-300 computer card (Becker & Hickl GmbH, Germany) provided the fast electronics for this measurement. The whole system fits neatly on a small cart for portability and to facilitate use in a clinical environment. The system is controlled from a flat-panel PC with a touch-sensitive screen. The system is intended either for surface measurements of time-resolved reflectance or for invasive measure-

ments by means of interstitial fibers inserted into the tissue.

The overall temporal response function of the system was approximately 100 ps (full width at half-maximum) when the average power after the fiber was tuned to approximately 2 mW. Tuning to higher power resulted in a broader response function. For tissues, these specifications give an optimal range of interfiber distances of approximately 1–2 cm. The measurements were performed at an interfiber distance of 15 mm. For each measurement, 100,000 counts were acquired.

B. Data Evaluation

We obtained the absorption and reduced scattering coefficients by fitting the solution of the diffusion equation for a semi-infinite homogenous medium, with the extrapolated boundary condition,[28] to the measured data. The diffusion coefficient, D, was assumed to be independent of the absorption of the medium; i.e., $D = 1/3\mu_s'$.[29] The theoretical curve was convolved with the instrumental transfer function, as measured with the source and the detector fiber facing each other, with collimating lenses to collect the light for the detector fiber. The resultant curve was fitted to the data over a range starting at 80% of the maximum intensity on the rising flank and ending at 1% on the trailing flank.[30] We accomplished the fit with a Levenberg–Marquardt algorithm[31] by varying μ_a and μ_s' to minimize χ^2.

4. Integrating-Sphere System

A. Optical Setup

The integrating-sphere setup was similar to the one described in Ref. 26, with a 75-W Xe lamp used as the light source. The sphere (Oriel Corporation, Stratford, Conn.) allows detection of total transmittance T and total reflectance R from a sample placed at either the entrance or the exit port. We guided the light to the sphere by using a 600 μm-diameter fiber and collimated it by using a lens and a pair of apertures. The light from the sphere was guided by an optical fiber bundle to a spectrometer (270M; SPEX Industries, Inc., Edison, N.J.). A cryocooled CCD camera (OMA-Vision; EG&G PARC, Princeton, N.J.) was used for detection. The collimated transmittance was measured in a separate setup in which a series of collinear apertures served to suppress the scattered light such that only the nonscattered light was collected by a fiber bundle guiding the light to the spectrometer. Attenuation filters were used to increase the dynamic range of this measurement, which yielded total attenuation coefficient $\mu_t = \mu_a + \mu_s$ from the Beer–Lambert law. To measure the epoxy phantoms we prepared 1.0-mm-thick slabs.

B. Determination of Optical Properties

We extracted the optical properties from the measured values R, T and μ_t, using an MPR method based on Monte Carlo simulations[27] that in principle was similar to the method used for the fiber-probe system. A previously computed database of R and T spanning the expected range of optical properties ($0 < \mu_a < 0.7\ \mathrm{cm}^{-1}$, $1 < \mu_s < 70\ \mathrm{cm}^{-1}$, $0.4 < g < 0.9$, $n = 1.55$) was fitted to a polynomial model. The properties μ_a, μ_s, and g were extracted from the model by a Newton–Raphson algorithm. Unlike in the method described in Ref. 27, which used a fixed value of g, three-dimensional rather than two-dimensional polynomials were used in the regression. Because of the limited sizes of the ports of the integrating sphere, there were losses of light at the outer parts of the sample. This effect was incorporated in to the Monte Carlo simulations, as otherwise the losses would have led to an overestimation of the absorption properties.[32] We accomplished this by incorporating the sphere entrance and exit port diameters in to the Monte Carlo simulations. For evaluation of tissue samples a different database was used ($0 < \mu_a < 0.5\ \mathrm{cm}^{-1}$, $5 < \mu_s < 120\ \mathrm{cm}^{-1}$, $0.8 < g < 0.995$, $n = 1.4$).

5. Test Samples

A. Solid Tissue Phantoms

Twenty-five phantoms were prepared from clear, solvent-free epoxy resin with an aliphatic amine as hardener (NM 500; Nils Malmgren AB, Ytterby, Sweden), according to the guidelines given by Firbank *et al.*[33,34] The epoxy had a pot life of ~6 h after the two components were mixed. TiO powder (T-8141; Sigma-Aldrich, St. Louis, Missouri) was used as a scatterer. Based on integrating-sphere measurements, TiO was found to give a reduced scattering coefficient μ_s' of approximately $6\ \mathrm{cm}^{-1}/(\mathrm{mg/g})$ at 785 nm when it was dispersed in the epoxy, linear to at least $30\ \mathrm{cm}^{-1}$. As absorbing pigment, toner from a copying machine was used; it had a fairly flat absorption spectrum throughout the visible and near-infrared regions. The toner also had some scattering characteristics, which means that the absorption coefficient is not trivially obtained from spectrophotometer readings alone. Again based on integrating-sphere measurements, the absorption coefficient of the toner dispersed in epoxy was found to be approximately $1\ \mathrm{cm}^{-1}/(\mathrm{mg/g})$ at 785 nm. A stock solution of hardener and toner (1.2 mg/g) was prepared for preparation of the phantom. The TiO was weighed directly for each phantom, with 1-mg accuracy. The concentrations of TiO and absorbing pigment are shown in Table 1. Cylindrical polypropylene cups were used as molds, resulting in phantoms with a diameter of 6.5 cm and a height of 5.5 cm. After hardening for 12 h at room temperature, the phantoms were hardened at 55 °C for 24 h, and then their upper surfaces were machined smooth. For the integrating-sphere measurements, cuvettes were made from microscope slides into which ~1 mL from each phantom was poured before the epoxy hardened, yielding 1.0-mm-thick samples, approximately 3 cm by 3 cm wide.

No settling of the TiO during the curing process was observed by other groups of researchers,[33] and by

Table 1. Concentrations of TiO and Black Pigment Added to the Phantoms

Phantom	Concentration
Increasing μ_s'	TiO (mg/g)
A	0.79
B	1.20
C	1.61
D	2.02
E	2.42
Increasing μ_a	Black pigment (μg/g)
1	6.4
2	13.8
3	21.1
4	28.5
5	35.9

visual inspection we could not detect any settling. However, in the slabs prepared for the integrating-sphere measurements, a weak curtain pattern was visible as the viscous resin was poured into the cuvette chamber. The implications of this pattern are discussed in Section 7 below.

B. Measurements of Pork Meat

Measurements of bone-free pork chops were made with all systems. The pork chops were purchased at the local supermarket on the same day as the measurements were made and were kept wrapped in plastic at room temperature for 3–4 h before the measurements. For the integrating-sphere measurements the meat was cut into 1.0-mm thick slices and placed between microscope slides, with pieces of slides used as spacers, and then clamped together.

C. *In vivo* Measurements

We also performed measurements on the insides of the forearms of two of the experimenters, using the spatially and time-resolved systems. The procedure was otherwise identical to the measurements of the phantoms.

6. Results

A. Solid Tissue Phantoms

A spectral characterization of the phantoms obtained from the integrating-sphere measurements is presented in Fig. 1. The spectra evaluated for μ_s' [Fig. 1(a)], μ_a [Fig. 1(b)], μ_s [Fig. 1 (c)], and g [Fig. 1 (d)] are shown as averages of the phantoms with equal amounts of scattering or absorption agents added. The absorption spectra [Fig. 1 (b)] were determined both by the added toner and by the intrinsic absorption of the epoxy resin.[34]

Figure 2 shows the values of μ_s' and μ_a obtained from each system for wavelength 660 nm. The results at 785 nm were similar, although the absolute values were shifted somewhat (data not shown).

The μ_s' values generally agreed within 10% among the systems, except for the row of lowest scattering (row A according to Table 1), where the fiber-probe and time-resolved data were as much as 35% lower than for the integrating sphere.

The values of μ_a are similar for the time-resolved and the integrating-sphere systems but are somewhat higher with the fiber-probe system. The integrating-sphere values are, however, more unevenly distributed, and there seems to be a trend toward lower values of μ_a for the phantoms with lower scattering (A and B), as we discuss in Section 7 below.

B. Pork Meat and In Vivo Measurements

The meat sample was included in the study as an example of realistic biological tissue. Nine measurements were performed with both the fiber-probe and the time-resolved systems at three positions, with the probes moved by ~0.5 cm between positions. For the integrating-sphere experiment, measurements of diffuse transmittance and reflectance were made on three samples. The results from the measurements are presented in Table 2. The fiber-probe measurements could vary by as much as a factor of 2 when the probe head was moved only ~1 cm, indicating that the sample was not particularly homogeneous even though it seemed so by visible inspection.

The time-and spatially resolved systems were tested on the forearms of two of the experimenters. Although *in vivo* measurements of the skin surface represent an inhomogeneous sampling volume, all measurements were nevertheless evaluated with the assumption of homogeneity. Three measurement at approximately the same position were performed. The results are presented in Table 3. The discrepancies between the systems are discussed in Section 7 below.

7. Discussion and Conclusion

The integrating-sphere method has a proven record of producing accurate values of the scattering coefficient, as verified by tests of polystyrene microspheres in water suspensions, for which the scattering could be calculated exactly from Mie theory.[27] The results from that investigation showed that the relative difference between the measured values of μ_s' and the predicted (by Mie theory) values of μ_s' was on average 1.7%. The method used to extract the optical properties, the MPR method based on Monte Carlo simulations, can also be regarded as state of the art in terms of inverse algorithms for integrating-sphere measurements.

The slabs designed for the integrating-sphere measurements are a potential source of error compared with the large phantoms, because the slabs exhibit slight inhomogeneities. When the slabs were inspected closely, weak curtain patterns were visible in them where the epoxy resin had been running down the sides of the glass cuvette. In preparing the phantoms we had taken much care to mix the resin and the scattering–absorbing agents both mechanically and by use of an ultrasonic bath, so we anticipate that the phantoms themselves were homogeneous. Deviations in the integrating-sphere results may

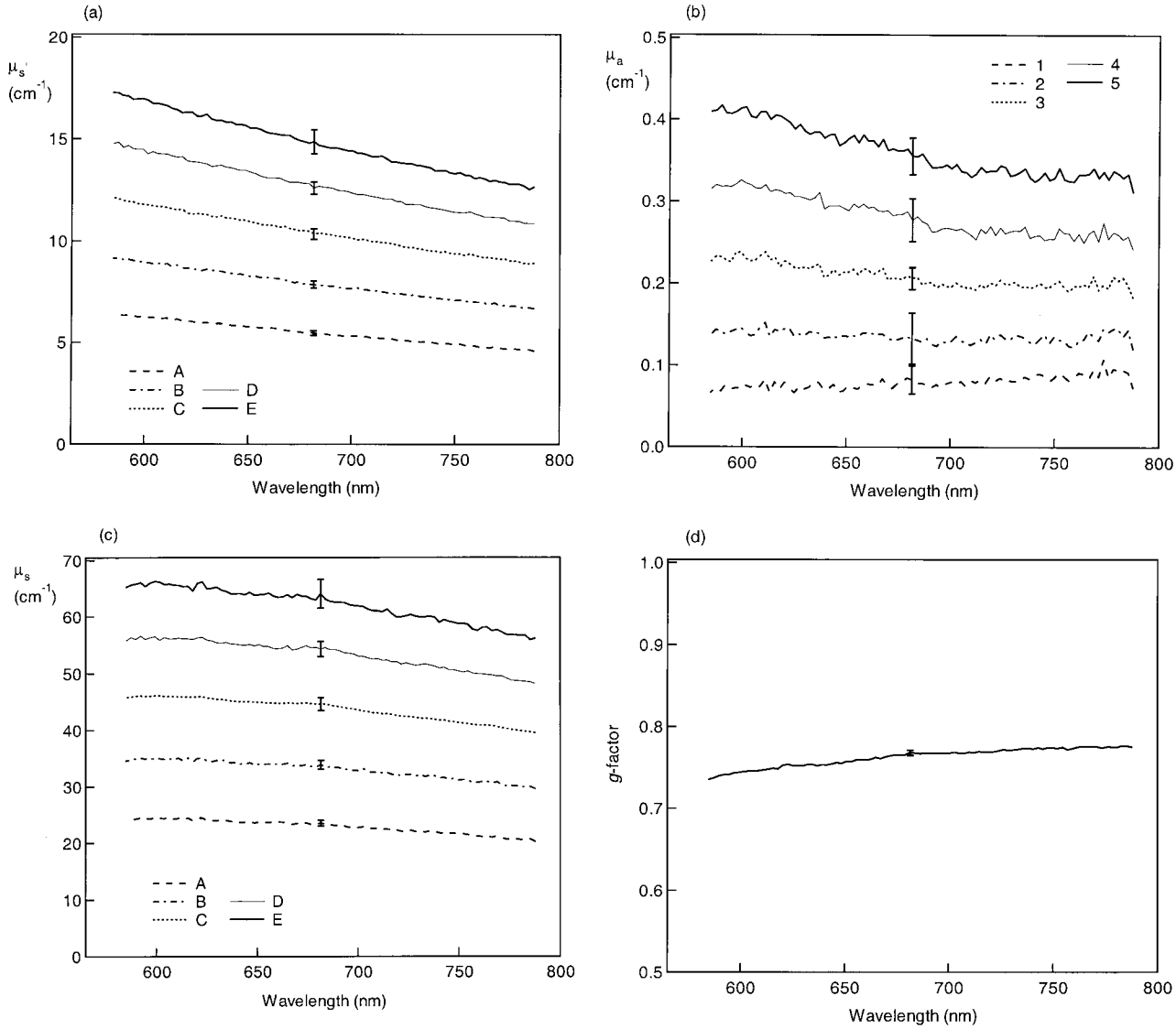

Fig. 1. Spectral characteristics of the phantoms as measured with the integrating sphere. (a) μ_s' spectra presented as averages of the phantoms with the same amount of TiO added, corresponding to A–E in Table 1. (b) μ_a spectra presented as averages of the 1–5 phantoms in Table 1. (c) μ_s spectra for A–E. The anisotropy factor g is presented in (d) as an average of all phantoms. Error bars represent one standard deviation.

thus also be the result of measuring not quite the same properties as in the bulk phantoms.

As we stated in Subsection 5.A, the toner had some scattering characteristics. However, they were negligible compared with the scattering from the TiO. No increase in the scattering coefficient could be observed when the concentration of toner was increased (Fig. 2), and it is clear from Table 1 that the concentration of toner was very low compared with that of TiO. The evaluation of the g factor [Fig. 1(d)] was of little importance for comparison with the other systems. However, the results may be of interest when one is discussing the merits of the integrating-sphere technique itself. In performing the μ_t measurement it is imperative that the amount of scattered light that is collected by the detector be negligible. The collimated beam setup was therefore rigorously characterized before being used, and we determined that attenuation coefficients of as much as 120 cm^{-1} could be measured with the setup, well above the numbers found in this study.

The absorption coefficients extracted by the integrating-sphere method deviated more among phantoms that should have the same properties, shown in Fig 2(f). This result was expected because the evaluation of μ_a is problematic when μ_a is low. Monte Carlo simulations showed that the difference between no black pigment and the lowest concentration of pigment corresponds to less than 1% difference in the measurement of R or T, and thus the evaluation is highly susceptible to measurement noise. A problem with integrating-sphere measurements in this respect is losses of light caused by the finite diameters of the sphere ports, which translate directly into an over-

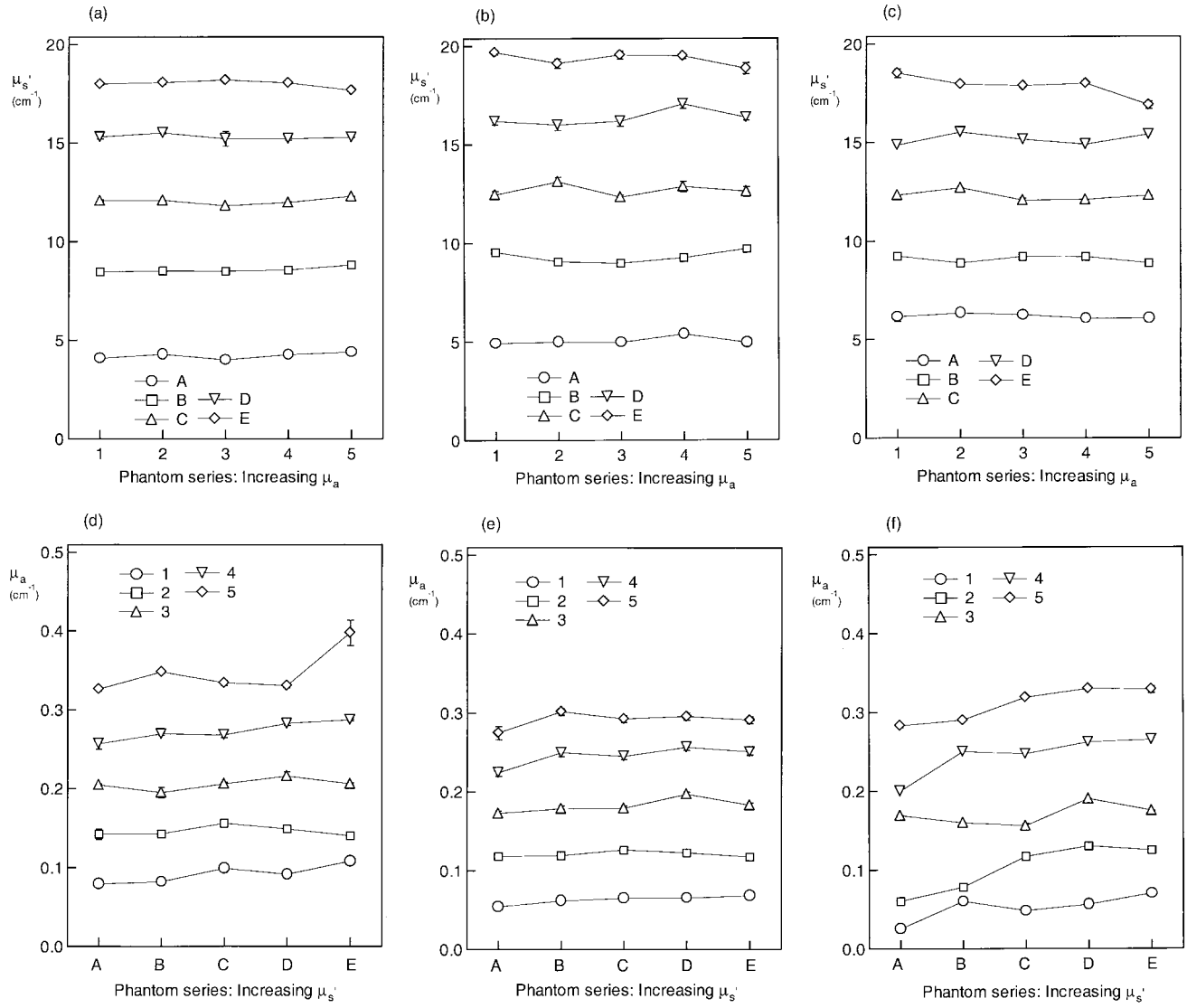

Fig. 2. Values of μ_s' and μ_a of the solid phantoms, as determined by the three systems, at 660 nm. The results are presented as functions of phantoms with the same amounts of TiO or black pigment added, according to Table 1. (a), (d) μ_s' and μ_a, respectively, from the fiber-probe system; (b), (e) corresponding results from the time-resolved system; (c), (f) corresponding results from the integrating-sphere system. Error bars represent one standard deviation for repeated measurements. Note that, for the integrating sphere, repeated measurements were performed only for phantoms A1, A5, C3, E1, and E5.

estimation of the absorption.[32] These losses, which can amount to 5% if the attenuation of the sample is low, were compensated for in the Monte Carlo model. In our setup the losses correspond to a detection limit of μ_a of $\sim$0.5 cm^{-1} if no correction is applied. If the true absorption coefficient is lower than this value, the losses will become the determining factor, and without corrections the evaluated value of μ_a can never be lower. However, even with corrections it is difficult to model the experimental conditions exactly, and the trend of lower values of μ_a for the low-scattering phantoms (A and B) is most likely an artifact that is due to

Table 2. Results of Measurements of the Meat Sample

	Fiber-Probe Method		Time-Resolved Method		Integrating-Sphere Method			
Property	μ_s' (cm^{-1})	μ_a (cm^{-1})	μ_s' (cm^{-1})	μ_a (cm^{-1})	μ_s' (cm^{-1})	μ_a (cm^{-1})	g	μ_s (cm^{-1})
Mean	6.9	0.043	6.6	0.037	4.9	0.061	0.94	82
Standard deviation	1.4	0.014	0.5	0.008	1.1	0.020	0.006	11

Table 3. Results of Measurements of Forearms of the Experimenters[a]

Person	Fiber-Probe Method μ_s'	Time-Resolved Method μ_s' (cm^{-1})
1	10.6	2.5
2	11.8	5.0

[a]For both persons, the fiber-probe method measured μ_a as 0.19 cm, and the time-resolved method measured μ_a as 0.20 cm.

the fact that the compensation in the Monte Carlo model was not exact. Nevertheless, the results show that the integrating-sphere method can produce useful results even for low-absorption coefficients, provided that proper compensation for losses is made. In this study the detection limit for μ_a was lowered an order of magnitude to $\sim 0.05\ cm^{-1}$.

The time-resolved method, however, produced an even distribution of μ_a for the low-absorption phantoms [Fig. 2(e)]. The slope of the trailing flank of the time-dispersion curve is determined largely by the absorption coefficient, and for low absorption the fit with the diffusion equation is fairly robust. Our conclusion is that the time-resolved technique is preferable when one is measuring low-absorption coefficients. Another interpretation is that the path length of the light is very long for the diffusely propagating light, which makes the measurement sensitive even to small absorption coefficients. The μ_a values for the highest concentration of absorber and the lowest amount of scatterer dip slightly compared with the rest, a result that can be explained by the fact that the diffusion approximation is starting to lose validity for those parameters. The fiber-probe system gave values of μ_a that were more evenly distributed than the integrating-sphere results [Fig. 2(d)]. The value for phantom E5 is likely an outlier, probably because of the low signal for this high-attenuation phantom. In as much as we calibrated the fiber system by utilizing a regression method, which tends to smooth irregularities in the calibration data, it is expected that the results will be more evenly distributed than the integrating-sphere results for μ_a. The absorption values are consistently higher for the fiber-probe system than for the other systems, which may be indicative of slight cross talk in the evaluation model, because the values of μ_s' are at the same time the lowest of the three systems.

As for scattering, the fiber-probe system yielded values of μ_s' within 5% of the integrating-sphere results [Figs. 2(a) and 2(c)], except for the row with the lowest scattering. During the experimental work it was apparent that the fiber-probe system had problems with low-scattering (below 5 cm^{-1}) coefficients. This may be attributed to the fixed detection distances. For low-scattering coefficients the probe would have needed to measure at longer distances to provide data for a robust evaluation. The scattering results for the time-resolved system look similar [Fig. 2(b)], and, again, it is apparent that the values of μ_s' are underestimated for low-scattering samples. In this case the reason can be attributed to the limited validity of the diffusion equation for this combination of μ_s', μ_a, and interfiber distance. The determination of μ_s' was somewhat sensitive to assumptions made in the fitting process. We achieved the best fit, in terms of the lowest value of χ^2, by allowing starting time t_0 of the time-dispersion curve to be a fitting parameter, together with μ_s' and μ_a. It is reasonable to be able to improve the fit by increasing the number of fitting parameters. However, it seems unphysical to have the starting time as a free parameter in the fitting procedure when the actual value of t_0 is known from the reference pulse in the measurement. Even though the χ^2 values were slightly worse for fitting with fixed t_0, the results obtained were closer to the integrating-sphere results. The results presented in this paper were thus obtained with a fixed value of t_0. Because it is known that the diffusion approximation is less accurate for early times, Cubeddu *et al.* used the 80% point of the rising flank of the curve as the starting point of the fitting and the 1% point of the trailing flank as the end point.[30] This approach was practiced in the study reported here too.

A general trend for the time-resolved data is that μ_s' is slightly higher and μ_a slightly lower than for the other systems. The reason for this systematic trend can probably be found in higher-order effects that are not accounted for by the diffusion approximation, i.e., most notably that the model is not accurate for early times. It has also been suggested that the radiative lifetimes (of the order of 100 fs) of the scattering events may have to be taken into account, which could explain the deviation trends in μ_s' and μ_a.[35]

The absolute accuracy of the fiber-probe system can be traced to the accuracy of the integrating-sphere measurements of the calibration set. The errors in the calibration set are comparable to the errors in the validation set measured with the integrating sphere, because the calibration set was made in an identical manner. However, the final calibration for the fiber-probe system is more accurate than the individual calibration points; this is a result of using the regression technique.[15]

The variation in the measurements of the meat sample is indicative of the heterogeneity of the sample and also reflects the different sampling volumes of the systems. The sampling depth depends critically on the interfiber distance between source and detector fiber.[36] The time-resolved system has the largest sampling volume and tends to average small variations. This phenomenon can be seen from Table 2, where the time-resolved system can be seen to exhibit the lowest standard deviations. The two other systems sample in millimeter-sized regions, and the results are thus more sensitive to small inhomogeneties, such as small streaks of fat or connective tissue. For the fiber probe the evaluation of the reduced scattering coefficient is especially sensitive to small inhomogeneities, as the scattering coefficient is determined primarily by the reflectance at the closest distance.[15]

One way to reduce sensitivity to small inhomogeneities and to noise in the detected signals when the

fiber-probe system is used was to use the signals from all detector distances rather than just two, as was done in previous studies. In principle, μ_a and μ_s' may be determined by use of $R(r)$ data from only two of the six detector distances of the fiber probe. A previous paper[15] reported application of the MPR technique to create a calibration model and subsequently to extract μ_a and μ_s' from $R(r)$ measurements at $r_1 = 0.6$ mm and at $r_2 = 7.8$ mm. As only two optical properties were extracted, i.e., μ_a and μ_s', the MPR method implies exactly two input variables as well, i.e., $R(r_1)$ and $R(r_2)$. In the research reported in this paper, all source–detector distances from the measurements were used. The number of independent signals was then reduced to two by application of principal-component analysis as a dimension reduction method.

As was pointed out above, the sampling volume in the *in vivo* skin measurements is inherently inhomogeneous, because the skin and the underlying tissues are a layered structure. This inhomogeneity would pose no problem in a comparison of the systems if the sampling volumes were the same, because the inhomogeneities would average out. Such is not the case here, however, as is obvious when one compares the measurement geometry of the time-and the spatially resolved systems. The 15-mm fiber spacing for the time-resolved system means that the detected light will have traveled along a deeper path than the detected light in the spatially resolved system.[36] For the spatially resolved system, the sampling depths will be different for the various radial distances. Also, as this system measures the diffuse reflectance for distances up to 7.8 mm from the source only, this method samples tissue layers at smaller depths than the time-resolved system. Most of the information about the scattering is, as mentioned above, collected at the first detector distance, at 0.6 mm, which means a very shallow sampling depth. In as much as skin and subcutaneous layers scatter more than muscle tissue, the spatially resolved systems consequently yielded higher values of μ_s' than the time-resolved systems (Table 2).

We included the meat sample and the *in vivo* measurements in our report as presented here to illustrate the performance of the systems in more-realistic measurement situations. Even in the relatively homogeneous meat sample, the results could vary by a factor of 2 for the fiber-probe system. The time-resolved method is the most robust in this respect, as small heterogeneities tend to average out. The discrepancies in the results point to one important observation, namely, that quantitative measurements of optical properties are sometimes impossible to perform if the assumption of homogeneous tissue is made. Only when the tissue can certainly be assumed to be homogeneous are such measurements useful. In other cases, either relative measurements, which may be system dependent, will have to suffice or one will have to utilize more-sophisticated inverse models based on assumptions of inhomogeneous tissue. Nevertheless, we have shown that when the requirement of a homogeneous medium is fulfilled, the three methods produce results for reduced scattering coefficient μ_s' that coincide with in 10% of one another over most of the relevant parameter space for biological soft tissue. The results for absorption are more complicated in terms of the relative errors, because the absorption coefficient in some tissues can be quite low. However, the differences in the evaluated absolute values for μ_a were within 0.05 cm^{-1} for the three measurement techniques.

We thank Antonio Pifferi (Department of Physics, Politecnicio di Milano, Milan, Italy) for the software used for the evaluation of the data recorded by the time-resolved system. In addition, we thank Claes af Klinteberg, Magnus Andersson, and Anders Nilsson for aiding us with the time-resolved measurements. We greatly appreciate help from Carsten Pedersen (Bang & Olufsen Medicom a/s, Struer, Denmark) in repairing the fiber probe system. This study was financially supported by European Commission grants QLG1-2000-00690 and QLG1-2000-01464 and by the Swedish Research Council.

References

1. R. Richards-Kortum and E. Sevick-Muraca, "Quantitative optical spectroscopy for tissue diagnosis," Annu. Rev. Phys. Chem. **47,** 555–606 (1996).
2. G. A. Wagnières, W. M. Star, and B. C. Wilson, "*In vivo* fluorescence spectroscopy and imaging for oncological applications," Photochem. Photobiol. **68,** 603–632 (1998).
3. G. J. Müller and A. Roggan, eds., *Laser-Induced Interstitial Thermotherapy* (SPIE Press, Bellingham, Wash., 1995).
4. K. Ivarsson, J. Olsrud, C. Sturesson, P. H. Möller, B. R. Persson, and K.-G. Tranberg, "Feedback interstitial diode laser (805 nm) thermotherapy system: *ex vivo* evaluation and mathematical modeling with one and four fibers," Lasers Surg. Med. **22,** 86–96 (1998).
5. A. M. K. Nilsson, R. Berg, and S. Andersson-Engels, "Measurements of the optical properties of tissue in conjunction with photodynamic therapy," Appl. Opt. **34,** 4609–4619 (1995).
6. T. Johansson, M. S. Thompson, M. Stenberg, C. af Klinteberg, S. Andersson-Engels, S. Svanberg, and K. Svanberg, "Feasibility study of a novel system for combined light dosimetry and interstitial photodynamic treatment of massive tumors," Appl. Opt. **41,** 1462–1468 (2002).
7. J. C. Hebden, H. Veenstra, H. Dehghani, E. M. C. Hillman, M. Schweiger, S. R. Arridge, and D. T. Delpy, "Three-dimensional time-resolved optical tomography of a conical breast phantom," Appl. Opt. **40,** 3278–3287 (2001).
8. C. H. Schmitz, M. Locker, J. M. Lasker, A. H. Hielscher, and R. L. Barbour, "Instrumentation for fast functional optical tomography," Rev. Sci. Instrum. **73,** 429–439 (2002).
9. T. J. Farrell, M. S. Patterson, and B. Wilson, "A diffusion theory model of spatially resolved, steady-state diffuse reflectance for noninvasive determination of tissue optical properties *in vivo*," Med. Phys. **19,** 879–888 (1992).
10. S. L. Jacques, A. Gutsche, J. Schwartz, L. Wang, and F. Tittel, "Video reflectometry to specify optical properties of tissue *in vivo*," in *Medical Optical Tomography: Functional Imaging and Monitoring*, G. J. Müller, B. Chance, R. R. Alfano, S. R. Arridge, J. Beuthan, E. Gratton, M. Kaschke, B. R. Masters, S. Svanberg, and P. van der Zee, eds. Vol. IS11 of SPIE Institute Series (SPIE Press, Bellingham, Wash. 1993), pp. 211–226.
11. A. Kienle, L. Lilge, M. S. Patterson, R. Hibst, R. Steiner, and

B. C. Wilson, "Spatially resolved absolute diffuse reflectance measurements for noninvasive determination of the optical scattering and absorption coefficients of biological tissue," Appl. Opt. **35,** 2304–2314 (1996).
12. R. Bays, G. Wagnières, D. Robert, D. Braichotte, J. F. Savary, P. Monnier, and H. van den Bergh, "Clinical determination of tissue optical properties by endoscopic spatially resolved reflectometry," Appl. Opt. **35,** 1756–1766 (1996).
13. R. M. P. Doornbos, R. Lang, M. C. Aalders, F. W. Cross, and H. J. C. M. Sterenborg, "The determination of *in vivo* human tissue optical properties and absolute chromophore concentrations using spatially resolved steady-state diffuse reflectance spectroscopy," Phys. Med. Biol. **44,** 967–981 (1999).
14. T. H. Pham, F. Bevilacqua, T. Spott, J. S. Dam, B. J. Tromberg, and S. Andersson-Engels, "Quantifying the absorption and reduced scattering coefficients of tissue-like turbid media over a broad spectral range using a non-contact Fourier interferometric, hyperspectral imaging system," Appl. Opt. **39,** 6487–6497 (2000).
15. J. S. Dam, C. B. Pedersen, T. Dalgaard, P. E. Fabricius, P. Aruna, and S. Andersson-Engels, "Fiber-optic probe for noninvasive real-time determination of tissue optical properties at multiple wavelengths," Appl. Opt. **40,** 1155–1164 (2001).
16. S. L. Jacques, "Time-resolved reflectance spectroscopy in turbid tissues," IEEE Trans. Biomed. Eng. **36,** 1155–1161 (1989).
17. S. Andersson-Engels, R. Berg, O. Jarlman, and S. Svanberg, "Time-resolved transillumination for medical diagnostics," Opt. Lett. **15,** 1179–1181 (1990).
18. M. Ferrari, Q. Wei, L. Carraresi, R. A. De Blasi, and G. Zaccanti, "Time-resolved spectroscopy of the human forearm," J. Photochem. Photobiol. B **16,** 141–153 (1992).
19. S. J. Madsen, B. C. Wilson, M. S. Patterson, Y. D. Park, S. L. Jacques, and Y. Hefetz, "Experimental tests of a simple diffusion model for the estimation of scattering and absorption coefficients of turbid media from time-resolved diffuse reflectance measure," Appl. Opt. **31,** 3509–3517 (1992).
20. K. Suzuki, Y. Yamashita, K. Ohta, and B. Chance, "Quantitative measurement of optical parameters in the breast using time-resolved spectroscopy. Phantom and preliminary *in vivo* results," Invest. Radiol. **29,** 410–414 (1994).
21. J. Kölzer, G. Mitic, J. Otto, and W. Zinth, "Measurements of the optical properties of breast tissue using time-resolved transillumination," in *Photon Transport in Highly Scattering Tissue*, S. Avrillier, B. Chance, G. J. Müller, A. V. Priezzhev, and V. V. Tuchin, eds., Proc. SPIE **2326,** 143–152 (1995).
22. X. Liang, L. Wang, P. P. Ho, and R. R. Alfano, "True scattering coefficients of turbid media," in *Optical Tomography, Photon Migration and Spectroscopy of Tissue and Model Media: Theory, Human Studies, and Instrumentation*, B. Chance and R. R. Alfano, eds., Proc. SPIE **2389,** 571–574 (1995).
23. R. Cubeddu, A. Pifferi, P. Taroni, A. Torricelli, and G. Valentini, "Noninvasive absorption and scattering spectroscopy of bulk diffusive media: an application to the optical characterization of human breast," Appl. Phys. Lett. **74,** 874–876 (1999).
24. J. W. Pickering, S. A. Prahl, N. van Wieringen, J. F. Beek, H. J. C. M. Sterenborg, and M. J. C. van Gemert, "Double-integrating-sphere system for measuring the optical properties of tissue," Appl. Opt. **32,** 399–410 (1993).
25. A. Roggan, H. J. Albrecht, K. Dörschel, O. Minet, and G. J. Müller, "Experimental set-up and Monte-Carlo model for the determination of optical tissue properties in the wavelength range 330–1100 nm," in *Laser Interaction with Hard and Soft Tissue II*, H. J. Albrecht, G. P. Delacretaz, T. H. Meier, R. W. Steiner, L. O. Svaasand, and M. J. van Gemert, eds., Proc. SPIE **2323,** 21–46 (1995).
26. A. M. K. Nilsson, C. Sturesson, D. L. Liu, and S. Andersson-Engels, "Changes in spectral shape of tissue optical properties in conjunction with laser-induced thermotherapy," Appl. Opt. **37,** 1256–1267 (1998).
27. J. S. Dam, T. Dalgaard, P. E. Fabricius, and S. Andersson-Engels, "Multiple polynomial regression method for determination of biomedical optical properties from integrating sphere measurements," Appl. Opt. **39,** 1202–1209 (2000).
28. R. C. Haskell, L. O. Svaasand, T.-T. Tsay, T.-C. Feng, M. S. McAdams, and B. J. Tromberg, "Boundary conditions for the diffusion equation in radiative transfer," J. Opt. Soc. Am. A **11,** 2727–2741 (1994).
29. K. Furutsu and Y. Yamada, "Diffusion approximation for a dissipative random medium and the applications," Phys. Rev. E **50,** 3634–3640 (1994).
30. R. Cubeddu, A. Pifferi, P. Taroni, A. Torricelli, and G. Valentini, "Experimental test of theoretical models for time-resolved reflectance," Med. Phys. **23,** 1625–1633 (1996).
31. W. H. Press, S. A. Teukolsky, W. T. Vetterling, and B. P. Flannery, *Numerical Recipes in C: The Art of Scientific Computing* (Cambridge U. Press, New York, 1992).
32. G. de Vries, J. F. Beek, G. W. Lucassen, and M. J. C. van Gemert, "The effect of light losses in double integrating spheres on optical properties estimation," IEEE J. Sel. Top. Quantum Electron. **5,** 944–947 (1999).
33. M. Firbank and D. T. Delpy, "A design for a stable and reproducible phantom for use in near infra-red imaging and spectroscopy," Phys. Med. Biol. **38,** 847–853 (1993).
34. M. Firbank, M. Oda, and D. T. Delpy, "An improved design for a stable and reproducable phantom material for use in near-infrared spectroscopy and imaging," Phys. Med. Biol. **40,** 955–961 (1995).
35. I. V. Yaroslavsky, A. N. Yaroslavsky, V. V. Tuchin, and H.-J. Schwarzmaier, "Effect of the scattering delay on time-dependent photon migration in turbid media," Appl. Opt. **36,** 6529–6538 (1997).
36. M. S. Patterson, S. Andersson-Engels, B. C. Wilson, and E. K. Osei, "Absorption spectroscopy in tissue-simulating materials: a theoretical and experimental study of photon paths," Appl. Opt. **34,** 22–30 (1995).